Identifying the Progenitor of Stellar Streams

URN: 6690310 Supervisor: D. Erkal
Department of Physics, University of Surrey, Guildford, GU2 7XH, UK

June 3, 2024

Abstract

Stellar streams, the remnants of tidally disrupted progenitor systems, provide a unique perspective on galactic evolution. This study focusses on stellar streams formed after the total dissolution of their progenitors, offering a comprehensive analysis of their dynamics. By integrating observational data with theoretical modelling, we investigated the properties and trajectories of dissolved progenitors, aiming to understand the mechanisms and evolutionary pathways underlying stream formation. Our research illuminates the intricate interplay between galactic dynamics and stellar evolution.

Through mock observations and simulations, we evaluate the reliability of methods for determining the original position of dissolved progenitors within stellar streams using density distributions. Although the goal is to identify the progenitor as a peak in density, our findings reveal a form of uncertainty stemming from multiple smaller peaks, attributed to variable rates of matter emission from the source, an uncertainty that will cause issues when applied to observational data where often only a partial fraction of the stream is observable. Computational simulations of mock streams enable us to explore the nature of stream evolution from progenitor dissolution to elongated streams. From our simulations, we also analyse how streams transform and the emission of stars and matter by progenitors throughout their lifetimes holds promise for uncovering the internal matter distribution of undisrupted globular clusters and dwarf galaxies.

1 Stellar Steams: A Synopsis

Stellar streams, a fundamental aspect of the galactic structure, offer significant insight into the hierarchical structure formation of galaxies. This process, motivated by the formation of smaller objects that merge to create larger entities such as dwarf galaxies, is a key factor in the evolution of galaxies. As these larger formations fall onto the Milky Way, they create stellar streams. These streams are composed of stars that exhibit shared kinematical and/or chemical properties (Newberg and Carlin, 2016), often observed as elongated overdensities in the stellar distribution, which are densities higher than the typical background (Carlberg, 2009).

Stellar streams arise from the tidal disruption of dwarf galaxies or globular clusters (Combes et al., 1999) as they orbit due to the gravitational potential of larger galaxies (Li et al., 2022) (Bonaca et al., 2021). The gravitational forces exerted by the host galaxy cause these progenitor systems to undergo tidal ripping, leading to the dissolution of their constituent stars along their orbital paths (Montanari and Garcia-Bellido, 2022) (Küpper et al., 2010). Consequently, the stars disperse along coherent trajectories, forming the characteristic elongated structures observed in stellar streams. These structures are composed of the stars that were once part of the original body, or progenitor. Now scattered along the orbital path of the progenitor, much like breadcrumbs left as traces. These huge stellar stream structures exhibit elliptical shapes and vary in density throughout their length. Stellar streams vary in size and length depending on their period of disruption, the size and distribution of mass in the progenitor, and the orbital path of the progenitor. Spanning a range of radial distances from the galactic centre from the order of a few to hundreds of kiloparsecs (kpc).

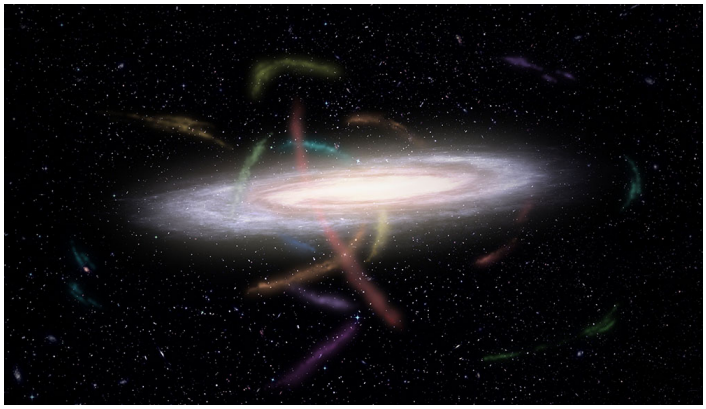

Figure 1: An artist's impression of a visual representation showing dozens of stellar streams surrounding our Milky Way Galaxy. Formed from dwarf galaxies and globular clusters as satellites, torn apart by our galaxy's gravity (Josephides and S5 Collaboration, 2022).

Stellar streams serve as repositories of crucial information regarding the assembly history of galaxies, as they retain imprints of their progenitor systems' orbital dynamics and chemical compositions (Newberg and Carlin, 2016) (Carlin et al., 2016). The study of these streams enables astronomers to trace the accretion events and mergers that have shaped the morphology and stellar content of galaxies over cosmic time (Panithanpaisal et al., 2021). Stellar streams serve as powerful probes for unveiling the presence and distribution of dark matter in galaxies (Banik et al., 2018) (Ibata et al., 2002). As these streams orbit within galactic potentials, they interact gravitationally with dark-matter halos, leaving distinct imprints on their trajectories and structures (McGee and Bonaca, 2022). Their orbital paths allow for the calculation of the gravitational potential of the main galaxy that the progenitor orbits and hence aid the understanding of the presence of dark-matter subhaloes.

The structure of stellar streams and their respective progenitor change as they evolve through time: Firstly, when less matter is located in the arms and the progenitor is still visible (Panithanpaisal et al., 2021). In this case, one can make direct measurements. Astronomers employ a combination of observational techniques and theoretical modelling to characterise the properties and elucidate their role in shaping the observed features of the stellar stream in question.

Imaging plays a crucial role in characterising stellar streams. Telescopes capture images of these streams, revealing the positions of stars in the sky and their colours. By analysing the distribution of stars, astronomers can infer the stream's shape, width, and density. In addition, imaging helps identify gaps or overdensities within the stream, which may indicate interactions with other objects or dark matter subhalos (Li et al., 2022). We interpret the observed image data using processes such as isochrone fitting, these being theoretical models that describe the evolution of stars in a stellar population. These models predict how the brightness and colour of stars change over time. Astronomers utilise observational data to extract colour and luminosity values, integrating them with theoretical models (the isochrones) that delineate the evolutionary courses of stars with various masses and ages. By aligning the isochrones with the observed colour-magnitude diagrams (CMDs) of stars within the stream, scientists determine the stream's age through comparative analysis. Additionally, isochrone fitting offers insights into the metallicity of the parent system (Mints and Hekker, 2018).

This process has been replaced by a faster and more accurate technique, now possible due to improvements in telescope and imaging technology. Telescopes like Gaia allow astronomers to measure the proper motions of stars—i.e., their actual velocities across the sky. Proper motions provide information about the stream's kinematics and orbital motion. Combining proper motions with radial velocities via Doppler redshifts enables the reconstruction of the full 3D velocity distribution of stars in the stream Li et al. (2022).

Imaging is used to determine the positions of stars in the sky and their colours. This helps us to understand the distribution and types of stars in a given region. Spectroscopy provides us with information about the velocity of stars along our line of sight and their chemical composition. Vital for understanding the movement and makeup of these celestial bodies (Mints and Hekker, 2018). Additionally, telescopes such as Gaia are used for determining proper motions, which are the actual velocities of stars across the sky (GAIA Collaboration, 2023).

Such methods are essential for the calculation of the structural and dynamical properties of the progenitor. Spectral analysis can be used to calculate the metallicities and elemental composition. Stellar age dating combines isochrone fitting with age-metallicity analysis (Angus et al., 2019). Age-metallicity analysis considers the relationship between a star's age and its metallicity. Young stars tend to be more metal rich (higher abundance of heavy elements) than older stars. By analysing the metallicity distribution of stars in the stream, astronomers estimate the age of the progenitor system. In conjunction with dynamical modelling techniques, such as orbit fitting and gravitational simulations, allow for the reconstruction of past trajectories of the system, and hence future estimations can also be made.

Secondly, as for a stream and progenitor system that has undergone significant evolution, the progenitor is often observed to have undergone complete dissolution, where almost all stars have left the progenitor's gravitational attraction. This means that it is no longer observable as a distinct entity. Such research into the whereabouts of a progenitor in a stellar stream is key as almost all observed streams belong to this category, that is, are not observed to have a clear observable source of stars (Mateu, 2023). Analysis of this type requires the use of indirect evidence and theoretical modelling, using the following steps. Firstly, applying observational constraints on the stream. In this case, despite the lack of a progenitor, the stellar stream infers a lot of key information about the former progenitor. By analysing the distribution of data of star positions and densities within the streams, it should be possible for one to calculate the tidal disruption history and orbital parameters of the system. Numerical simulations of galactic evolution can be used to generate predictions for the formation and evolution of the streams in different scenarios (Shipp et al., 2023), compare them with other systems, and assess the likelihood of each scenario. The analysis allows us to estimate the mass, size, and orbit of the progenitor system based on the imprint on the observed stellar stream.

2 Method Part 1: Proper motion

2.1 Aims

This project will undergo an analysis of when the progenitor is no longer visible, where the computational analysis will be tested to determine the accuracy of the simulations. Firstly, the theory that the use of density fluctuations is a viable method of progenitor analysis will be performed on systems where the progenitor has not dissolved, to test the sturdiness and reliability of the computational model. Assuming that the results can be deemed sufficiently accurate, further analysis making use of the same technique will be implemented for those stellar streams whose progenitor has undergone complete dissolution.

Understanding the location of progenitors is crucial, yet it can be challenging. Stellar streams consist of stars that are farther away than those within the Milky Way. Consequently, their magnitudes are often very small, making them difficult to detect. GAIA Collaboration (2023), launched in 2013, represents the best current full-sky survey capable of scanning the entire sky to a depth of apparent magnitude (G = 20.7). However, this lack of desired depth means that more limited sky surveys, such as the Dark Energy Survey DES Collaboration (2021), which can reach depths exceeding 24, a factor of over 20 times fainter, provide the ability to detect far more stars within these streams and measure their corresponding angular velocity. The trade-off is a reduced field of view for detection.

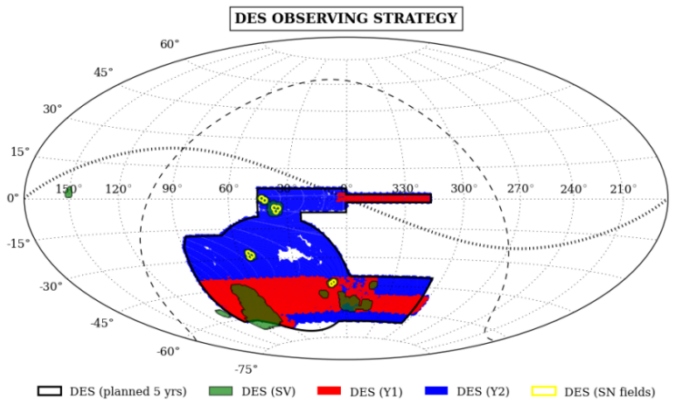

Figure 2: A figure showing the limited region of sky that has been observed to an incredible resolution and depth from DES (Abbott et al., 2016).

Additionally, the density of dust and gas in the central Milky Way plane obstructs observations, limiting the portion of a stream that can be measured. Despite these challenges, we hope that our technique will yield a progenitor position via a density function, we theorise an ideal result being a symmetric density distribution of stars within the observed range. This distribution could then be extrapolated to locate the progenitor before or after its dissolution, even when the region of the sky containing it is not visible.

The ability to pinpoint the location of the progenitor would facilitate a complete understanding of its numerous internal and external properties. Internally, we anticipate the presence of characteristics such as metallicity and mass gradients (Sharda et al., 2021). This implies that the composition of stars within the progenitor varies as a function of the radial distance from their centres. This is analogous to the Milky Way (Ness and Freeman, 2016), where the stars in the spiral arms exhibit a distinctive metallicity gradient. These stars are typically more metal-rich towards the galactic centre, reflecting the higher amounts of stellar recycling. This gradient becomes less pronounced as we move outward, signifying a decrease in the frequency of newer, metal-poor stars.

In understanding the tidal disruption and ripping of the data, we could attempt to understand from the stars observed in the streams the distribution of different matter in the globular cluster or dwarf galaxy before the disruption. Externally by locating the progenitor, we can attempt to understand from the movement of the stellar streams arms the distribution of mass around the orbited galaxy, and hence calculate a value of invisible dark matter in the outer regions of the galaxy.

2.2 Rotation and Transformation of Stellar Stream Data

Stellar stream data are acquired through a variety of methods. Among these techniques, the most prevalent currently involves the use of velocity data. Using the measurement of the velocities of stars within a stellar stream, astronomers can infer crucial information about its composition, origin, and evolution. This approach allows them to map out the trajectory of the stream and analyse its kinematics, shedding light on its formation mechanisms and interactions with the surrounding galactic environment.

In this paper, we will be making use of simulated streams, such that the method can be rigorously tested and parameters changed to ensure that no external factors are manipulating the results. If the technique is sufficient for simulated data we intend to apply it to true observation sky survey data to test if the model accuracy is upheld. Using a stream comprised of 10000 stars for a globular cluster. The first step is to observe a stellar stream in a Cartesian coordinate system:

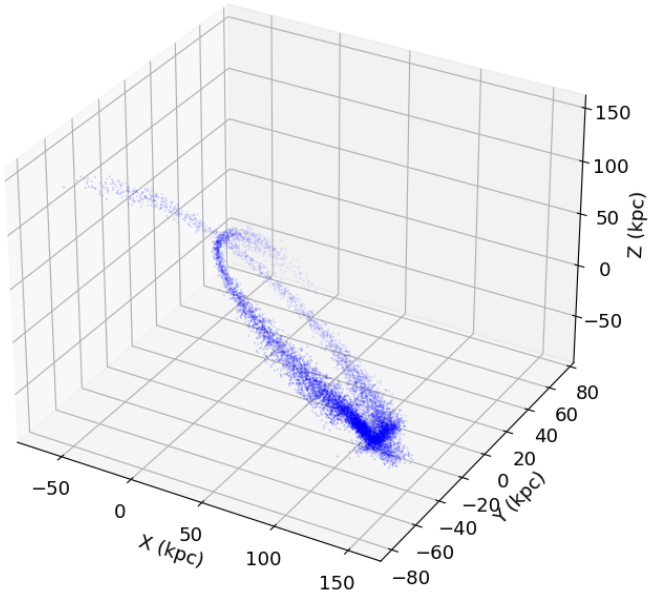

Figure 3: A plot to show a simulated stream composed of 10,000 stars for a globular cluster simulated for 6 Gyr from initial disruption. Where the simulation still has a clear progenitor position.

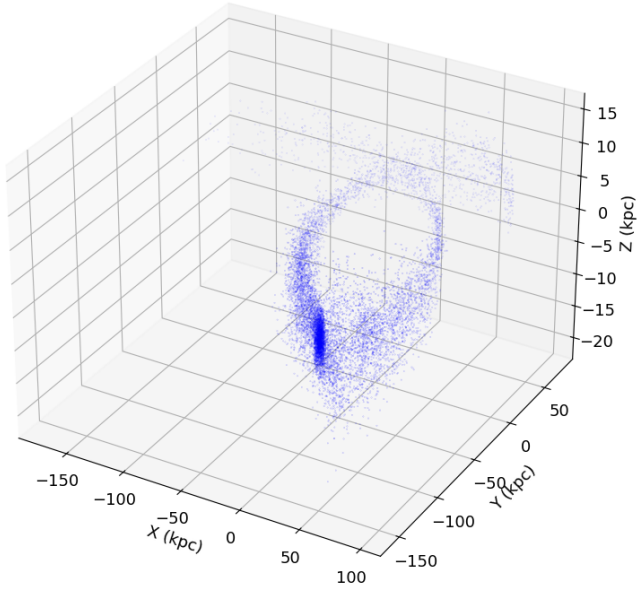

Figure 4: A plot showing the effects of the minimise function in finding an optimal angle for the rotation matrices to transform the stream into the X-Y plane. Noticing the scales of the axis, where the data spans huge distances in the X-Y plane where the distribution of matter in Z is contained within ±10kpc of the Z = 0.

To begin the investigation of the viability of using densities as a method to identify progenitors of stellar streams we need to find the spread of positions of the stars in the streams, making use of a proposed method such as in Koposov et al. (2023). This requires manipulating coordinates to align the stream with a plane that rotates to the **x** axis, achieved using a rotation matrix. The rotation matrix used in this process is given by:

$$R_{xy} = \begin{bmatrix} \cos(\theta) & 0 & -\sin(\theta) \\ 0 & 1 & 0 \\ \sin(\theta) & 0 & \cos(\theta) \end{bmatrix} \quad (1)$$

Here θ represents the rotation angle. Similarly, we utilised another rotation matrix R_{xy} for additional rotation around the **z**-axis, given by:

$$R_{xz} = \begin{bmatrix} \cos(\alpha) & -\sin(\alpha) & 0 \\ \sin(\alpha) & \cos(\alpha) & 0 \\ 0 & 0 & 1 \end{bmatrix} \quad (2)$$

The stream data was transformed using these rotation matrices sequentially, first applying R_{xy} and then R_{xz}, to align the stream approximately along the **xy**-plane. The angles θ and α were optimised by minimising the squared sum of the **z**-coordinates after rotation.

Before we apply the rotation to the stream, we subtract the observational position of an **x**-direction, so that we are working from the reference frame from which the origin at (0,0,0) is that of the galactic centre. Plotting the data results in a distribution we observe:

The result showed a distribution of data, we expect that regions closer to the progenitor will have a higher density, this is an observed general trend. However, the effects defied in Kepler's laws of motion are also exhibited. where the velocity of a star orbiting will undergo a deceleration when at apsides (the farthest point in the orbit about the primary body), resulting in a higher density. An acceleration at periapsis (the closest point in the orbit about the primary body) results in a lower density of stars.

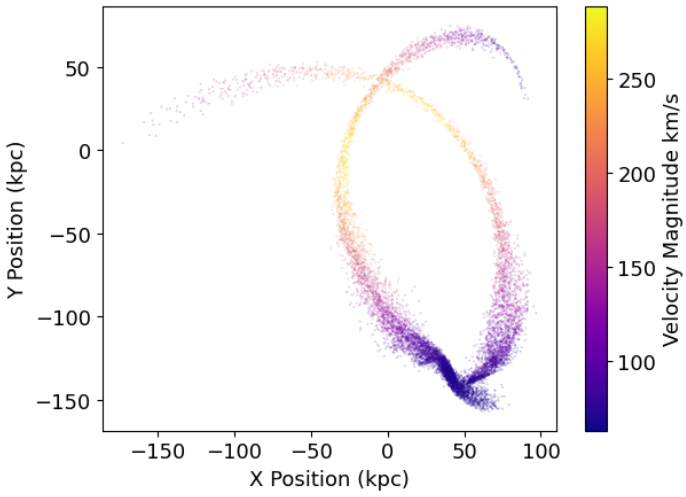

Figure 5: A plot to demonstrate the velocity of stars within the stream and its effects of causing "clumping" of stars when stars slow across their orbital path as they reach the furthest point from the central gravitational potential and they have been moving in opposition to this gravitational attraction.

It is important to note that for our density distribution to achieve the best possible results must implement a correction for this effect as the method only achieves ideal results in the case where the stream is unperturbed.

Cases for streams such as the Sagittarius stream where the stream has been perturbed by the gravitational influence of external mass (Vasiliev et al., 2020), in this case, the Large Magellanic Clouds will result in a non-uniform distribution (Shipp et al., 2021). Once again another limiting factor that might distort results when our density method is applied to observational data of many of the 12 Milky Way stellar streams, and potentially many more of other galaxies if they contain similar structures.

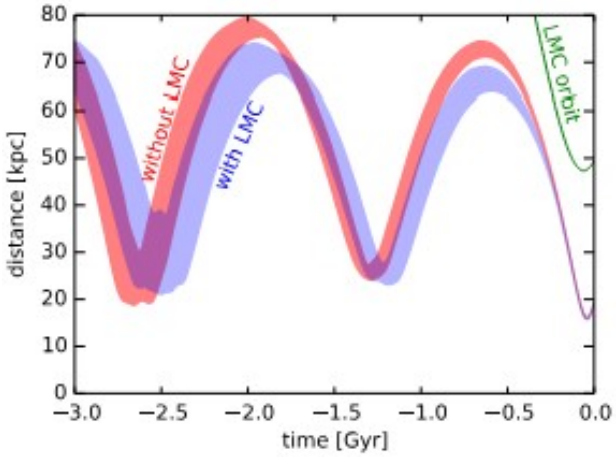

Figure 6: A figure showing how the research of simulations by Vasiliev et al. (2020) showed how satellite galaxies (Large Magellanic Clouds) might influence the orbital paths of stellar streams.

2.3 Filtering of Outliers

As seen in the figures the Stellar Stream used in the analysis is not a perfect closed elliptical orbital path. It has distinct tails; for the sake of the analysis of the Progenitor of the Stream, it is deemed imperative to remove these stars from the file as their phase angle will be the same as stars that have a closer position to the progenitor but have different velocities and will distort the density distribution, affecting the ability to observe trends in the data.

This process was achieved simply by applying a statistical Z score to the data and choosing a threshold such that only these tails were removed as observed. To achieve this the data was condensed onto a two-dimensional axis where values of **Z** were set to zero. The removal of the Z-score could be performed.

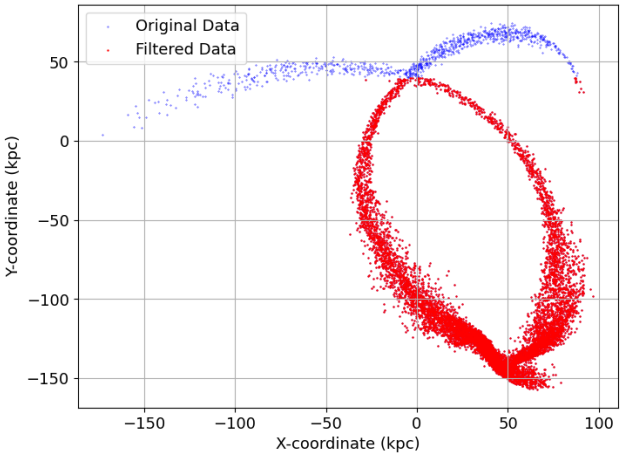

Figure 7: A plot showing the effects of the Z-scale threshold removal of the two tails in the extremities of the stream.

For this particular stream, a threshold value of 2.05 achieved the best results; however, for more complex streams a more manual method of point subtraction may need to be implemented.

Such processes might follow a process of finding a curve that fits the distribution and obtaining an angle for each star based on the star's nearest point to the curve.

In an ideal case where the progenitor position is not identifiable, we would not want to remove any data points from our data set. Hence if this technique were to be applied to observational data, an algorithm would need to be adopted such that the constituent stars of the stream could be unwrapped and assigned an angle of greater magnitude than the range $(-\pi, \pi)$.

2.4 Changing Coordinate system

From now for the sake of simplicity, we should transform to a spherical coordinate system, where we denote ϕ_1 as the azimuthal angle and ϕ_2 as the inclination. Computed using the transformations as follows:

$$\begin{aligned} \phi_1 &= \arctan\left(\frac{y}{x}\right) \\ \phi_2 &= \arcsin\left(\frac{z}{\sqrt{x^2+y^2+z^2}}\right) \end{aligned} \tag{3}$$

Then we wish to centre the data on the median value of ϕ_1. We denote the median value as ψ and use this angle to apply a new rotation:

$$\text{Rot} = \begin{bmatrix} \cos(\psi) & \sin(\psi) & 0 \\ -\sin(\psi) & \cos(\psi) & 0 \\ 0 & 0 & 1 \end{bmatrix} \tag{4}$$

To the data achieving transformations by the equations:

$$\begin{aligned} \phi_1 &= x \cdot \cos(\psi) + y \cdot \sin(\psi) \\ \phi_2 &= -x \cdot \sin(\psi) + y \cdot \cos(\psi) \\ z' &= z \end{aligned} \tag{5}$$

And by plotting we observe the spread of data in a spherical two-dimensional plane of ϕ_1 against ϕ_2 such that the data is centred about the point $\phi_1 = 0$.

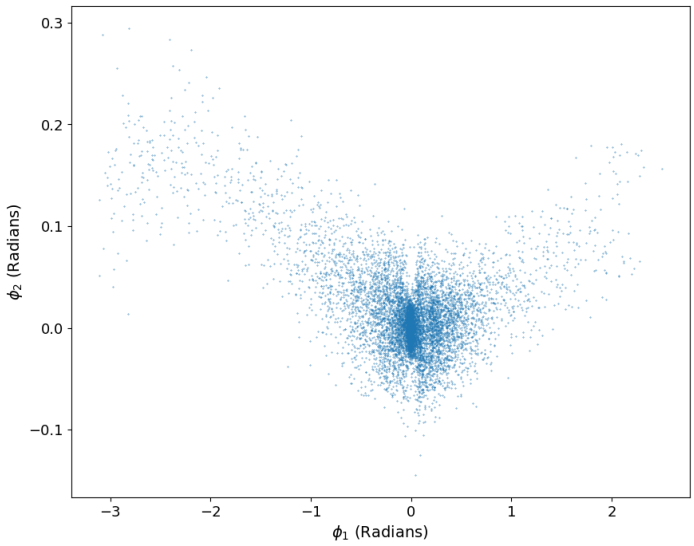

Figure 8: A plot showing the effects after the transform and centring of the data in an Azimuthal and Inclination-based plane.

2.5 Proper Motion

We account for the effects of modulations in velocity throughout the orbital path such that we can find the true density across the stream. We aim to find the proper motion of the stars within the stream, where proper motion refers to the apparent angular motion of a star across the sky relative to distant background objects. This is caused by its actual motion through space relative to the observer, and in the case of our observational data, we work from within the reference point of the telescope (or Earth). Using the chain rule, we have already found ϕ_1. We can easily find the derivative of the term $\frac{dN}{d\phi_1}$. The chain rule equation is given by:

$$\frac{dN}{dt} = \frac{dN}{d\phi_1} \cdot \frac{d\phi_1}{dt} \tag{6}$$

Where:

- $\frac{dN}{d\phi_1}$ represents the density distribution already found from matrix rotation.
- $\frac{d\phi_1}{dt}$ represents the proper motion, which has yet to be found.

Where if we multiply the density of stars in $d\phi_1$ by the newly found proper motion, we see that we derive a value $\frac{dN}{dt}$. This will represent an unperturbed density of stars in the case that there was no velocity fluctuation throughout the orbital path.

The proper motions could be computed by making use of the velocity data, a transformation matrix to convert from an equatorial-based longitude/ latitude to a right ascension/ declination coordinate system:

$$\mathbf{a_g} = \begin{bmatrix} -0.0548756 & +0.4941094 & -0.8676662 \\ -0.8734371 & -0.4448296 & -0.1980764 \\ -0.4838350 & 0.7469822 & +0.4559838 \end{bmatrix} \tag{7}$$

The Galactic and Equatorial coordinate systems are two different ways of mapping celestial objects. In the Galactic system, the symbols l and b represent Galactic longitude and latitude, respectively. The Galactic system is centred on the Sun, with the Galactic plane defined by the plane of the Milky Way. The zero point of Galactic longitude is the direction from the Sun to the centre of the Milky Way. Both Galactic longitude and latitude are measured in radians.

On the other hand, the Equatorial system uses Right Ascension (RA) and Declination (Dec). The equatorial system is based on the Earth's rotation axis, with the poles defined by the Earth's North and South poles and the equator by the Earth's equator. The zero point of RA is the vernal equinox (the point where the Sun crosses the celestial equator from the south to the north). RA is measured in time units, while Dec is measured in radians.

The Equatorial system is more commonly used for Earth-based observations, while the Galactic system is useful for studying the structure of our galaxy, hence why applying this transformation is useful as we wish to move to a galactic-centred reference point.

Initially, the velocity data of the stars is separated into its constituent components, in three-dimensional space. These components represent the velocities of the stars along the $\mathbf{x}$, $\mathbf{y}$, and $\mathbf{z}$ axes, providing information about their movement in space.

A transformation matrix $\mathbf{a_g}$ is then defined to facilitate the coordinate transformations. This matrix operates the role of rotating, scaling, and reorientation of the velocity vectors. By applying this transformation matrix to the velocity data, the code ensures that the subsequent calculations are performed in the new coordinate system.

After applying the transformation matrix, I proceeded to compute the observed positions and velocities of the stars. The data were taken to account for various factors, including the observer's location, the distance of the stars from the observer, and the relative motion between the observer and the stars. By incorporating these factors into the calculations, the code determines the observed positions and velocities of the stars as they would appear from the vantage point of the observer.

With the observed positions and velocities obtained, the code proceeds to calculate the proper motions of the stars, for this step, code from Denis Erkal (b) was helpfully supplied for the proper motion calculation in full.

Once calculated the proper motions could be plotted as a function of Φ's:

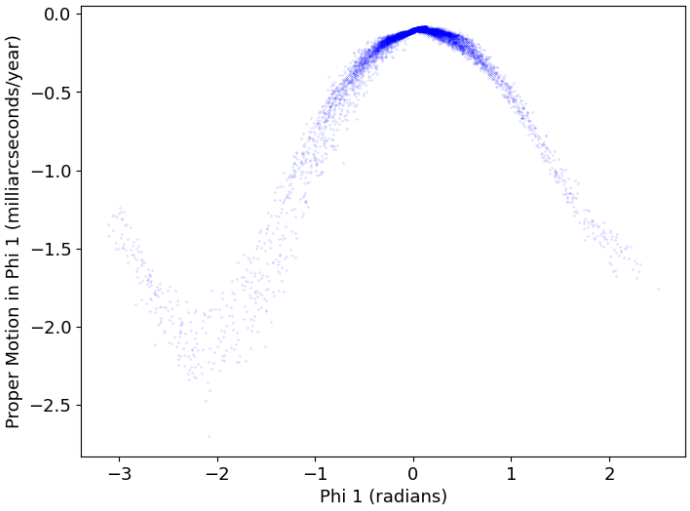

Figure 9: A plot showing the variation in proper motion of a stream aligned across the azimuthal axis.

2.6 Densities

To calculate the unperturbed densities in the stream we need to multiply as seen before the proper motion by the density distribution. Correcting for the aforementioned changes in velocity and its subsequent distortion effects on the density distribution. We create a histogram as a form of the density function of collective bins for phi coordinates and find the mean values of the proper motion in each bin. By multiplying these terms together we create a corrected number density accounting for the density we can analyse.

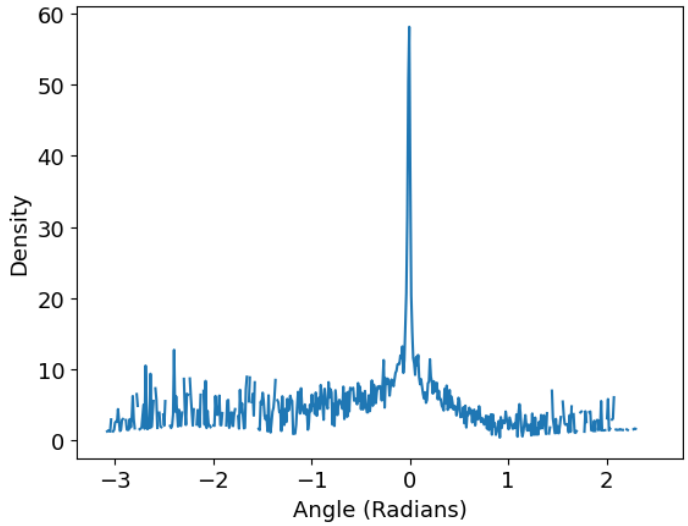

Figure 10: A plot to demonstrate the corrected number density distribution of stars across azimuthal angle.

2.7 Viability

Now that the model has been created, we need to analyse the results; we hope to see that the distribution of data in our plots is close to symmetric. Whilst we do see a clear peak denoting the progenitor position. The density distribution is not as clear as we would have hoped, with a higher weighting of densities in bins located to the left of the progenitor location at 0.

The results whilst they do contain clear evidence of noise, the peak of this stream is pronounced sufficiently such that the method could be used to identify the progenitor location.

Approximating a normal distribution to fit the main peak, we can obtain a peak location and uncertainty using the full-width half-maxima (FWHM) technique for the obtained location at an angle:

$$\text{Location of Progenitor} : -0.0087\,\text{Radians}$$
$$\text{Error (FWHM)} : \pm 0.0013\,\text{Radians}$$

However, these results might imply that, despite the method working for a stream early in its evolution, where the progenitor is visible. We might expect that the longer the stream is evolved the more distortion in our results and hence the difficulty of identifying the progenitor becomes.

3 Method Part 2: Snapshots

Having assessed whether the posited technique of utilising corrected densities is viable in providing insight into the progenitor's location prior to disruption was complete, Proceeding with the undertaking of understanding how the dissolution of progenitors occurs and whether the technique would uphold its ability to locate the progenitor post disruption. Making use of a computed N-body simulation of tidal disruption of a collection of bound stars. I processed the elongation of the stream over regular time steps to observe the events that occurred. The following analysis was performed.

3.1 Shrinking Sphere Approach

The sphere reduction approach aims to estimate the centroid position of a stellar stream by iteratively reducing the search space within spheres of decreasing radii centred around the stream. Given a set of stellar positions **P**, the algorithm proceeds as follows: starting with an initial search radius **R**, the median centre **C** of the stellar positions are computed. The points within a radius sphere **R** centred at **C** are then selected, and the median centre is recomputed based on these points. This process is repeated, with **R** halved at each iteration, until a minimum radius is reached. At each iteration, the median centre is updated on the basis of the points within the current sphere. Here, the initial radius **R** was a value that encapsulated all of the stars 256 kpc. A final value to provide a high degree of precision of 1 kpc was chosen as suitable.

3.2 Rotation Step

After estimating the centroid position using the sphere reduction approach, a rotation step is performed to align the stellar stream with a reference frame. This step involves finding the angle of rotation $\boldsymbol{\theta}$ such that the final progenitor position after sphere reduction lies on the **x** axis. The rotation matrix $\mathbf{R}_{xy}$ was used to rotate the points in the **xy** plane (1).

The rotation matrix is applied to the progenitor positions, resulting in a rotated configuration aligned with the **x**-axis.

3.3 Phase Step

The subsequent task involved coding to assign a phase angle to each star, an angle calculated from the degrees in radians from the progenitor about the origin. This involved applying a mask to the rotated stream to track when each star's angle traversed the quadrant from $\frac{\pi}{2}$ to $-\frac{\pi}{2}$, or vice versa in the opposite direction, between snapshots. In such instances, a 2π angle adjustment was applied to the star's phase angle. This allows for clear visualisation of the stellar stream by overlaying it with a colour map.

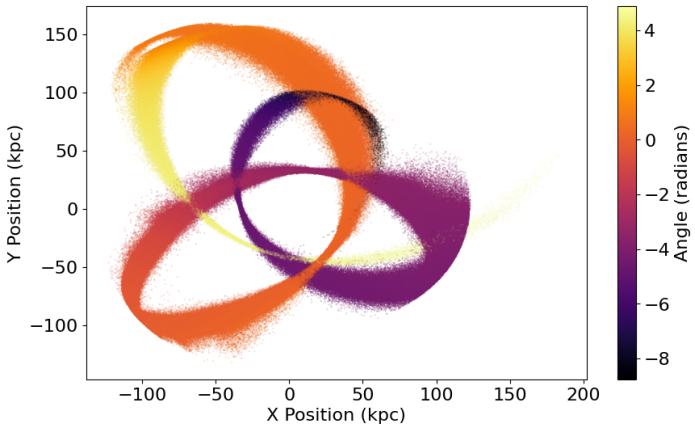

Figure 11: A plot to demonstrate the wrapping method on a snapshot. Showing how the new technique allows for unwrapping the stream in excess of the $-\pi$ to π range.

3.4 Progenitor Identification and Dissolution

When running this code, it is clear that there becomes a given snapshot where the wrapping code no longer provides accurate results. This occurs when the progenitor dissipates and so the coded reducing sphere approach is no longer an adequate technique. It is this point that we aim to understand.

We can attempt to continue using this technique if we attempt to follow the last stars that are located inside the progenitor up to the point where the stream ceases to exist at the final sufficient snapshot. keeping track of the IDs.

3.5 Densities Part 2

Likewise, as completed in Section 1, we can plot density distributions in azimuthal coordinates to gauge the progenitor location in the stream for all the snapshots, this time instead of tracking as a function of ϕ_1, we can track the density across the range of phases.

We apply the proper motion as a weighting, the weights are calculated using the ratio of proper motion to the cosine of the angle as follows.

$$\frac{\text{proper motion in l}}{\cos(b)}$$

The angle b represents the direction of observation. The projected proper motion is given by the equation takes into account the angle of observation.

Applying this to the density distribution, we observe a shift as follows:

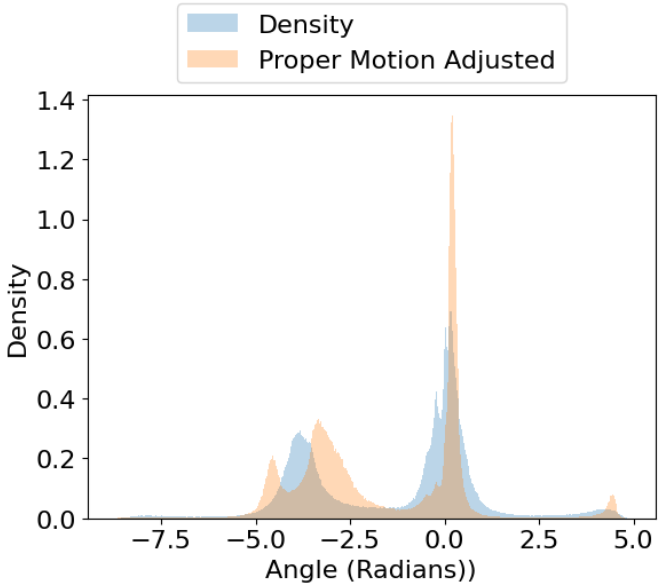

Figure 12: A plot to show the corrected densities of phase angles after proper motion is applied. Observing how the initial density distribution across angular position in blue, is shifted by the proper motion as shown in orange. Where the second peak at an angle of -4 radians caused by the bunching at apsides is changed significantly by the correction.

The symmetry that was present on the prior attempt for an early snapshot of a stream is no longer present. Consequently, the methodology employed in this research does not appear to be a viable approach for locating progenitors within stellar streams. It becomes challenging to assert with confidence whether a peak in density observed within a stream region accurately represents the progenitor or merely a false maximum. So, the hypothesis that identifying the progenitors becomes more difficult with time seems true.

3.6 Identifying Reasons for Failure

Initially, we embarked on this research with the expectation that our chosen technique would yield precise results. However, this assumption proved incorrect. Therefore, the logical next step is to investigate the underlying reasons for the unexpected outcomes.

Our first analytical step involved exploring the possibility of secondary and tertiary matter expulsions resulting from tidal forces, which may have influenced the expected outcomes. To accomplish this, we identified the snapshot corresponding to the departure of each star in the stream from the progenitor, defined within a region of 1kpc around the current progenitor position. Following this, we overlaid this data to discern any instances where the material was expelled from the progenitor at later stages in the stream's evolution.

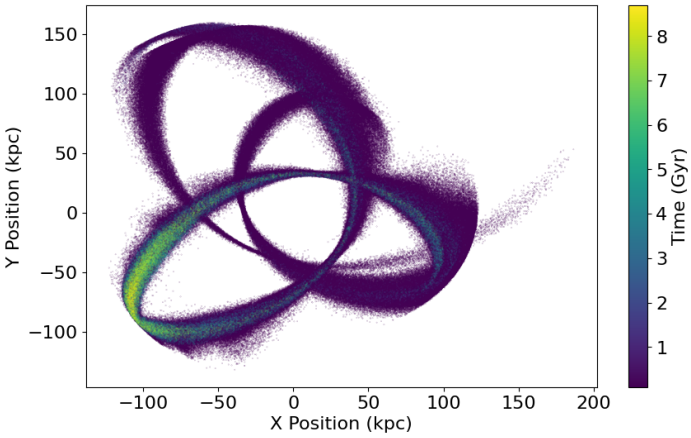

Figure 13: A plot to show the snapshots in which the stars left from a 1kpc radius of progenitor position. Observing how the majority of matter leaves at the earliest point in the initial tear, followed by secondary, tertiary, and subsequent ripping events in subsequent periapsis points in the progenitor's orbit path.

These results show clear evidence that a second if not multiple expulsion of matter has occurred in the simulated data, hence we have reasoning as to why our method failed.

To check the number of events and how the quantities of matter emitted in each event vary, we can plot the rates of matter emission out of the progenitor as a function of the snapshot where these events occur. For additional insight, including the distance from the progenitor to the central potential. We expect to observe that these events coincide with when the progenitor reaches its periapsis point:

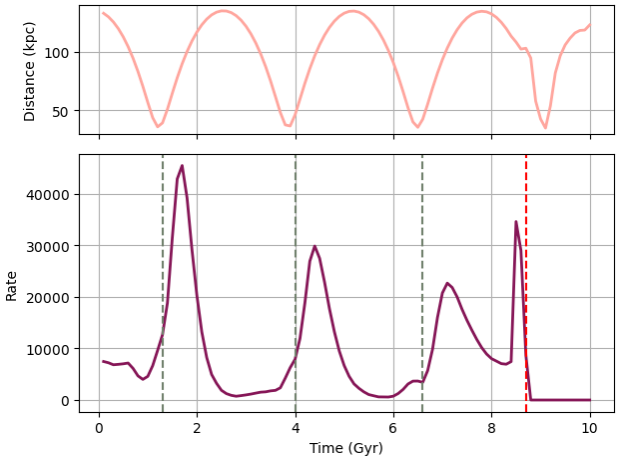

Figure 14: A plot to show the rates of matter emitted in particles per snapshot across the evolution and how these expulsion events coincide with the orbital path of the progenitor. Note that the number of stars released in each event decreases as fewer stars remain in the progenitor to be ripped. The dotted line in red signifies the failure point in the simulation shrinking sphere approach hence all stars are falsely recorded to have left.

This figure shows at least three clear events disregarding the initial tear at t = 0 to maintaina reasonable scale for subsequent events, in which the magnitude of these decreases as fewer stars are left in the progenitor. It is also clear how these events coincide with the periapsis, where there is an observed lag time between the point of closest approach and when stars leave. This is due for the stars take significant time to move from their position in the progenitor and cross the defined 5 kpc region which we define as the threshold for progenitor size.

We observe at a time of 8.4 Gyr, highlighted in red, how large amounts of stars are recorded to have left the defined radius around the shrinking sphere approach; this coaligns with the first snapshot in which the shrinking sphere approach fails, and hence all stars that have not left are incorrectly labelled to have left. From this point onwards it is clear that the results obtained from approximate unwrapping have the potential to return incorrect results; such occurrences become more exaggerated and frequent as the simulation continues.

Following the observed spread of data throughout the stream, as depicted in *Figure 13*, we note a correlation between a star's position in the stream and the timing of its expulsion. Stars that have been exposed to the stream for a longer duration tend to travel over larger angular distances from their original positions. To substantiate this initial observation, we generated a plot of the density distribution. The data was filtered based on the time of star expulsion, utilising our previous findings to establish intervals corresponding to expulsion events.

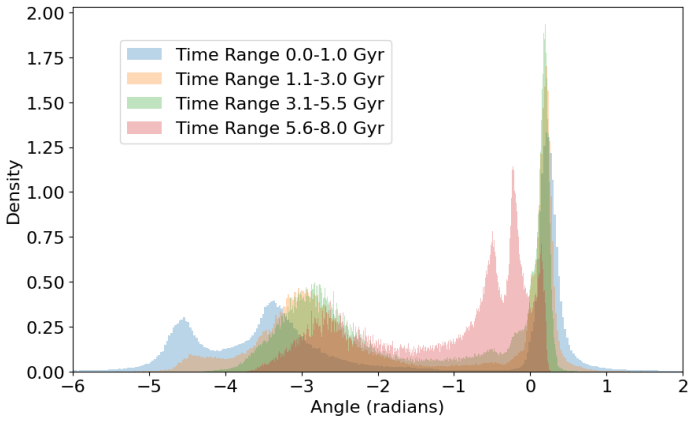

Figure 15: A plot to show the corrected densities of phase angles after proper motion is applied over a range of different snapshot ranges. Demonstrating how angles increase the longer stars have been in the stellar stream arms. Where each defined period in time is chosen based on a single disruption event of the progenitor.

We observe that the peaks co-align with specific snapshot times that match the times when the progenitor was located in proximity to the periapsis position. And so it seems the peaks are in correspondence to the uneven rates of progenitor disruption, and times when the progenitor is far from this location result in a flatter distribution and lower amounts of stars. We also observe how the correlation for where the longer stars have been outside the progenitor is higher than the angle at which they have been shifted. It seems that this is the main reason for failure in our technique as it would only be expected to work well for systems that experience a near-constant rate of stars leaving the progenitor. Such cases are few and far between, and so it seems unlikely that such a method will ever be adopted.

3.7 Constant Separation

As a proof of constant that the theory would work if stars were expelled at a constant rate from the progenitor, we set up a similar simulation where the rate of matter leaving is separated by a regular time interval. i.e. where the value of $\frac{dN}{dt}$ is constant throughout, the results obtained verify our theory where the resulting distribution of matter is constant. Therefore if this was the case the only deviation from this flat density distribution would be at the exact position of the progenitor where the density is attributed to the remaining stars left in the progenitor.

3.8 Potential future research

Despite the failure of the method, the results obtained reveal a key property that could be investigated separately, where the understanding that the matter in the streams is distributed over a wider range of angles the longer since the matter was expelled. Therefore assuming that the tidal disruption of the progenitor causes stars in the outer layers to shed first, one could investigate the variation of mass, age, and metallicity as a function of angle to create a cross-section of these dwarf galaxies and their constituent matter gradients before disruption.

3.9 Dwarf Galaxy

The simulated data we have been working on to this point are simulated with only baryonic matter; however, if we use a simulation where interactions due to dark matter are included. We hypothesise that these interactions might stabilise the rate at which matter is being expelled from the progenitor due to the lessening of the comparative magnitude of gravitational potential from the galactic centre. Hence, we hope that performing the prior code on the new system may result in better results.

When passing the new simulated data over the same timescale of 140 snapshots with 100 mega-year intervals through the same analysis, we observe a notably different result, the data spreads over a much higher angle, and as expected the stability of decay of the progenitor is improved, so much though that after the simulation timescale the progenitor can still be located by the method of reducing spheres, these results are shared by the density approach were we observe a distribution still plagued by unwanted peaks due to uneven rate off matter leaving the progenitor, but when proper motion is applied it attempts to correct for the effects and results in a far smoother and more symmetric distribution than the non-dark matter case.

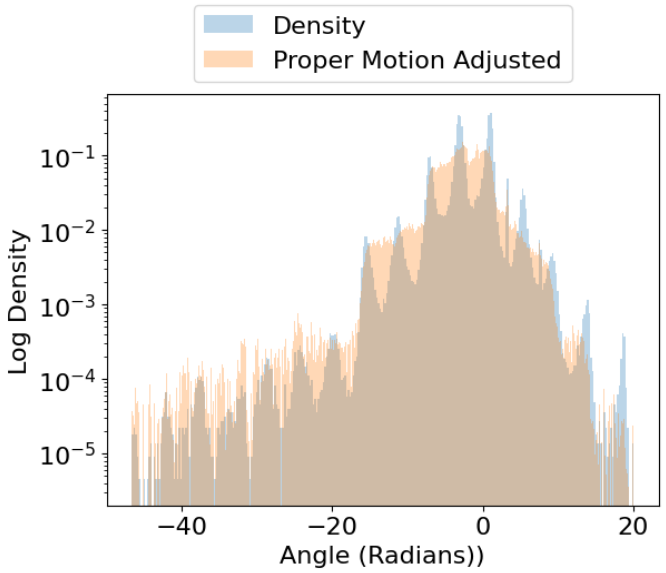

Figure 16: Graph showing density disruption of a Disrupted stream constrained by the presence of dark matter. Make note of the periodic blue peaks caused by the clumping and stretching of stars from velocity changes in orbit, which is corrected for as seen in orange.

4 After Disruption

4.1 Post disruption evolution

In our snapshot model, we can run to find the frame in time before the code can no longer find the progenitor with any certainty that such a value for our globular cluster simulation occurs at 12 Gyr after the initial ripping. This unique event, only possible due to the simulation format provides the possibility to track the final stars that are located within the progenitor moments before it dissipates and becomes untraceable. By keeping a note of these particular stars we can plot their paths in the later snapshots we can attempt to perceive what happens when the progenitor. For the non-dark matter simulation, we achieve the following:

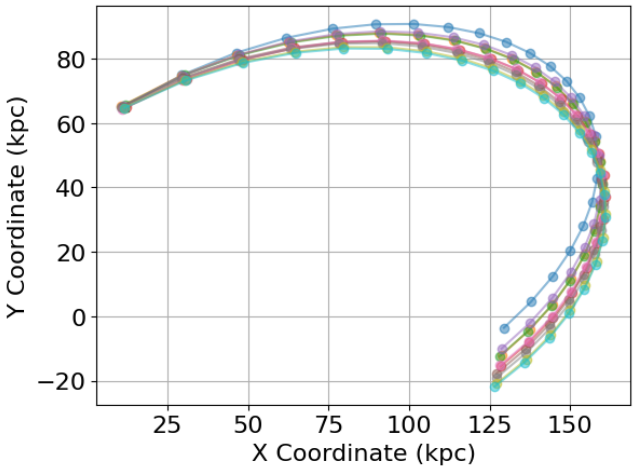

Figure 17: A plot to show the motion of stars in progenitor moments before dissolution. Where all initial stars are measured within a 1kpc region of the shrinking sphere approach, and we trace their identities across the following 20 Gyr to gauge what happens to the progenitor after the failure of our prior methodology.

We observe that stars that were initially just 1kpc from the progenitor position, after the progenitor ceases to exist, start to spread, reaching upward of 20kpc by the 14 Gyr.

Hence we can understand why the method of progenitor finding fails, sadly due to the failure of the rate of matter emitted plot after 8.5 Gyr as shown in figure *Figure 14* we do not have exact knowledge if this time scale aligns with a periapsis point and hence a disruption event. Therefore we have to make assumptions from the periodic nature of orbits, and from our data, we see an even rate of periapsis at intervals of approximately every 2.5 Gyr. A simple extrapolation of this period from the last major disruption of matter event gives the following predictions as 9.6 and 12.2 Gyr. The latter is a value close to the point in time where the identification fails. It seems reasonable to infer from these results that the cause of the failure is that for our simulation there becomes a point where so few stars are located in the progenitor after 6 ripping events that a direct measurement cannot identify the position.

4.2 Evolution of streams

To understand the dissolution of the progenitor we need to investigate the dispassion of matter over time achieved best by plotting all the evolutionary phases of the stream at intervals and observing when different surges of matter are expelled from the centre of the stream.

Figure 18 located in the appendix shows how by 1.5 Gyr snapshot the majority of the matter once located in the progenitor has already been expelled to form the main arm of the stream, these continue to elongate as tidal forces act on them, following which by the 4.5 Gyr snapshot we observe new matter leaving the stream, angled at a slightly different angle to the current arms, and elongate along a slightly different path, most clearly seen in snapshot 60 where left of the progenitor are located two separate arms of colour indicating the difference in snapshot were this matter was dispelled. A tertiary expulsion has occurred by the time of the 7.5 Gyr snapshot. Matter continues to leave the progenitor up to the point that the progenitor dissipates.

In our simulations, matter is initially pulled in the direction of gravitational tidal forces, which act perpendicular to the velocity of the progenitor's orbit. The stars, now in free space, maintain an orbital velocity similar to that of the progenitor from which they were emitted. As a result, the stars that were torn from the near side of the progenitor, now on a shorter orbital radius, move ahead of the progenitor, forming the arms in front of it. Conversely, the stars emitted from the far side end up on a larger radius and a longer orbital path, causing them to lag behind the progenitor.

We've also observed an interesting asymmetry in our stellar streams. In all of our simulations, the distribution of emitted matter is uneven on either side of the progenitor position. Specifically, the negative phase angles consistently have a higher density than the positive angles. This could be because, in all our simulations, the progenitor orbits clockwise. Therefore, the stars that are further along in their orbit (at a more advanced hour angle) are on a path with a smaller radius, which also happens to be a region of higher density. This asymmetry can be explained by the stronger gravitational pull of the tidal forces on the side of the stream closer to the potential (the advanced stream arm), compared to the side that's further away (the lagged stream arm).

5 Summary and Conclusions

In this study of Stellar Streams, we sought to answer whether the posited idea of the use of density would suffice sufficient results to locate the former progenitor position, once torn by tidal forces.

After employing various methodologies and analysing multiple data sets, we have determined that the conditions necessary for a density-based approach to yield consistently accurate results without any risk of false positives are exceedingly rare.

The techniques only worked in systems where the tidal disruption has been occurring for relatively shorter cosmic scales of time. For our simulations of a globular cluster any simulation time over 5 Gyr the method was no longer sufficiently accurate in the absence of dark matter. Following this, a simulation of dwarf galaxies was run, and the time for which the progenitor could be easily measured was increased after introducing sufficient dark matter such that the amount of matter shed in the initial tidal ripping was halved. However, once the system evolved to the point that the sphere reduction approach no longer obtained a sufficiently accurate value, the density distribution also failed to determine a clear progenitor position. The density results were corrected by applying a proper motion correction based on the angular velocities of the stars. This correction was hoped to flatten any irrelevant peaks in the distribution from the bunching at apsides and thinning at periapsis however whilst it did improve results, the density distributions after complete disruptions did not have the desired clarity such that we could apply this technique to observational data.

The failure of this method stemmed from the variable stripping rate of matter from the progenitor core. Expulsion events only occur in high numbers at points where the progenitor orbited in proximity to the periapsis point in the stream's orbit of the galactic gravitational potential. The requirements for the density function to remain near constant outside of the progenitor position were shown to require a constant rate of expulsion. And unlike the proper motion correction, there is no possible technique that can be used to account for this.

The longer that matter had been exposed away from the progenitor the greater angles it had shifted and the more likely the density distribution was to deviate from an ideal symmetric function.

The implementation of dark matter halos around the galaxy did result in improvements in the results, therefore much for this matter's presence in the interstellar medium the tidal ripping might be delayed. Identification of a progenitor may be possible. However, the more time passed since the progenitor could no longer be directly measured, the increased likelihood that the density method would not be able to achieve clear results.

There seems to be no way to remedy the issues with a density-based approach. Therefore, one has to rely on finding a stream where the tidal disruption rate is near constant. Such chances are slim and hence this technique is unlikely to have application for any great use in research. Even more so when sky surveys of adequate depth have limited scanning area of the sky and the disruption of clear observation of any streams that pass through the main body of gas and dust contained in the plane of the milky-way across our night sky.

We conducted an investigation into the asymmetry of matter distributions in our two evolved streams over 14 Gyr. Our analysis led to the conclusion that the asymmetry arises from variations in gravitational attraction strength on either side of the progenitor. Consequently, more matter is observed in the arm that precedes the progenitor, as material is pulled from the closer side onto a smaller orbital radius. Another factor contributing to difficulty in identifying the progenitor position with accuracy.

The setback and failure of our methodology did not go in vain; although our findings did not solve the initial problem, they hold promise in paving the way for future research avenues. We postulated that the potential for the use of tracing the temporal displacement of matter from earlier disruptions in the stellar stream to its current position could reveal valuable insights. Our simulations indicated that material emitted during earlier epochs tended to be located at greater angular distances from the progenitor. Moreover, if our hypothesis holds, that dwarf galaxies and globular clusters exhibit mass and age gradients before disruption, then the shedding of matter in layers during variable ripping at periapsis could result in observable composition gradients in the unwinding arms of the stream. Consequently, stellar streams might offer a means to dissect the internal composition of satellite dwarf galaxies and globular clusters orbiting a larger galactic mass.

6 Acknowledgements

I would like to express my sincere appreciation to Denis Erkal (a) for his invaluable guidance, support, and encouragement throughout the completion of my final-year project. His expertise, dedication, and constructive feedback have been instrumental in shaping the outcome of this work. I am deeply grateful for his mentorship and commitment to my academic growth.

References

T. Abbott, F. B. Abdalla, J. Aleksic´, S. Allam, A. Amara, D. Bacon, E. Balbinot, M. Banerji, K. Bechtol, A. Benoit-Levy ´, G. M. Bernstein, E. Bertin, J. Blazek, C. Bonnett, S. Bridle, D. Brooks, R. J. Brunner, E. BuckleyGeer, D. L. Burke, G. B. Caminha, D. Capozzi, J. Carlsen, A. Carnero-Rosell, M. Carollo, M. Carrasco-Kind, J. Carretero, F. J. Castander, L. Clerkin, T. Collett, C. Conselice, M. Crocce, C. E. Cunha, C. B. D'Andrea, L. N. da Costa, T. M. Davis, S. Desai, H. T. Diehl, J. P. Dietrich, S. Dodelson, P. Doel, A. Drlica-Wagner, J. Estrada, J. Etherington, A. E. Evrard, J. Fabbri, D. A. Finley, B. Flaugher, R. J. Foley, P. Fosalba, J. Frieman, J. Garc´ıa-Bellido, E. Gaztanaga, D. W. Gerdes, T. Giannantonio, D. A. Goldstein, D. Gruen, R. A. Gruendl, P. Guarnieri, G. Gutierrez, W. Hartley, K. Honscheid, B. Jain, D. J. James, T. Jeltema, S. Jouvel, R. Kessler, A. King, D. Kirk, R. Kron, K. Kuehn, N. Kuropatkin, O. Lahav, T. S. Li, M. Lima, H. Lin, M. A. G. Maia, M. Makler, M. Manera, C. Maraston, J. L. Marshall, P. Martini, R. G. McMahon, P. Melchior, A. Merson, C. J. Miller, R. Miquel, J. J. Mohr, X. Morice-Atkinson, K. Naidoo, E. Neilsen, R. C. Nichol, B. Nord, R. Ogando, F. Ostrovski, A. Palmese, A. Papadopoulos, H. V. Peiris, J. Peoples, W. J. Percival, A. A. Plazas, S. L. Reed, A. Refregier, A. K. Romer, A. Roodman, A. Ross, E. Rozo, E. S. Rykoff, I. Sadeh, M. Sako, C. Sanchez ´, E. Sanchez, B. Santiago, V. Scarpine, M. Schubnell, I. SevillaNoarbe, E. Sheldon, M. Smith, R. C. Smith, M. Soares-Santos, F. Sobreira, M. Soumagnac, E. Suchyta, M. Sullivan, M. Swanson, G. Tarle, J. Thaler, D. Thomas, R. C. Thomas, D. Tucker, J. D. Vieira, V. Vikram, A. R. Walker, R. H. Wechsler, J. Weller, W. Wester, L. Whiteway, H. Wilcox, B. Yanny, Y. Zhang, and J. Zuntz. The dark energy survey: more than dark energy - an overview. *Monthly Notices of the Royal Astronomical Society, Volume 460, Issue 2, 01 August 2016, Pages 1270–1299*, 2016. https://doi.org/10.48550/arXiv.1601.00329.

R. Angus, T. D. Morton, D. Foreman-Mackey, J. Van Saders, J. Curtis, S. R. Kane, M. Bedell, R. Kiman, D. W. Hogg, and J. Brewer. Toward precise stellar ages: Combining isochrone fitting with empirical gyrochronology. *The Astronomical Journal, Volume 158, Number 5*, 2019. https://doi.org/10.3847/1538-3881/ab3c53.

N. Banik, G. Bertone, J.Bovy, and N. Bozorgnia. Probing the nature of dark matter particles with stellar streams. *Submitted to Journal of Cosmology and Astroparticle Physics (JCAP)*, 2018. https://doi.org/10.48550/arXiv.1804.04384.

A. Bonaca, R. Naidu, C. Conroy, N. Caldwell, P. Cargile, J.J. Han, B. Johnson, J.M. Kruijssen, G. Myeong, J. Speagle, Y. S. Ting, and D. Zaritsky. Orbital clustering identifies the origins of galactic stellar streams. *The Astrophysical Journal Letters, Volume 909, Number 2*, 2021. https://dx.doi.org/10.3847/2041-8213/abeaa9.

R. G . Carlberg. Star stream folding by dark galactic subhaloes. *The Astrophysical Journal Letters, Volume 705, Number 2*, 2009. https://dx.doi.org/10.1088/0004-637X/705/2/L2.

J. L Carlin, R. L. Beaton, D. Martinez-Delgado, and R. J. Gabany. Stellar tidal streams in external galaxies. 2016. https://doi.org/10.48550/arXiv.1603.04656.

F. Combes, S. Leon, and G. Meylan. N-body simulations of globular cluster tides. *Astronomy and Astrophysics, v.352, p.149-162*, 1999. https://dx.doi.org/10.48550/arXiv.astro-ph/9910148.

DES Collaboration. Dark energy survey year 3 results: Photometric data set for cosmology. 2021. https://arxiv.org/pdf/2011.03407.pdf.

D. Erkal. https://personalpages.surrey.ac.uk/d.erkal/, a.

D. Erkal. Proper motion rotation matrix. https://github.com/derkal/Rotation-Matrix, b.

GAIA Collaboration. GAIA data release 3. *The Astronomical Journal, Volume 923, Number 2*, 2023. https://www.cosmos.esa.int/web/gaia/data-release-3.

R. A. Ibata, G. F. Lewis, M. J. Irwin, and T. Quinn. Uncovering cold dark matter halo substructure with tidal streams. *Monthly Notices of the Royal Astronomical Society, Volume 332, Issue 4, pp. 915-920*, 2002. https://doi.org/10.1046/j.1365-8711.2002.05358.x.

J. Josephides and S5 Collaboration. Stellar streams are revealing their secrets. 2022. https://skyandtelescope.org/astronomy-news/stellar-streams-are-revealing-their-secrets/.

S. E. Koposov, D. Erkal, T.S. Li, G. S. Da Costa, L. R. Cullinane, A. P. Ji, K. Kuehn, G. A. Lewis, A. B. Pace, N. Shipp, D. B. Zucker, J. Bland-Hawthorn, S. Lilleengen, S. L. Martell, and S5 Collaboration. Streams on fire: Populations of detectable stellar streams in the milky way and fire. *Monthly Notices of the Royal Astronomical Society, Volume 521, Issue 4, pp.4936-4962*, 2023. 10.48550/arXiv.2211.04495.

A. H. W. Küpper, P. Kroupa, H. Baumgardt, and D. C. Heggie. Tidal tails of star clusters. *Monthly Notices of the Royal Astronomical Society, Volume 401, Issue 1, pp. 105-120*, 2010. https://doi.org/10.1111/j.1365-2966.2009.15690.x.

T. S. Li, A. P. Ji, A. B. Pace, D. Erkal, S. E. Koposov, N. Shipp, G. S. Da Costa, L. R. Cullinane, K. Kuehn, G. F. Lewis, D. Mackey, J. D. Simpson, D. B. Zucker, P. S. Ferguson, S. L. Martell, J. Bland-Hawthorn, E. Balbinot, K. Tavangar, A. Drlica-Wagner, G. M. De Silva, J. D. Simon, and (S5 Collaboration). S5: The orbital and chemical properties of one dozen stellar streams. *The Astrophysics Journal, Volume 928, Number 1*, 2022. https://dx.doi.org/10.3847/1538-4357/ac46d3.

C. Mateu. galstreams: A library of milky way stellar stream footprints and tracks. *Monthly Notices of the Royal Astronomical Society, Volume 520, Issue 4, pp.5225-5258*, 2023. https://doi.org/10.1093/mnras/stad321.

C. McGee and A. Bonaca. Dark matter accounts for perturbation in the gd-1 stellar stream. 2022. https://doi.org/10.48550/arXiv.2104.09660.

A. Mints and S. Hekker. Isochrone fitting in the gaia era. *Astronomy and Astrophysics, Volume 618*, 2018. https://doi.org/10.1051/0004-6361/201832739.

F. Montanari and J. Garcia-Bellido. Mass classification of dark matter perturbers of stellar tidal streams. *Physics of the Dark Universe, Volume 35*, 2022. https://doi.org/10.1016/j.dark.2022.100978.

NASA/IPAC. Nasa/ipac extra-galactic database. https://ned.ipac.caltech.edu/.

M. Ness and K. Freeman. The metallicity distribution of the milky way bulge. *Published in Publications of the Astronomical Society of Australia, Volume 33, id.e022.*, 2016. https://arxiv.org/abs/1511.07438.

H. Newberg and J. Carlin. *Tidal Streams in the Local Group and Beyond*. 2016.

N. Panithanpaisal, R. E. Sanderson, A. Wetzel, E. C. Cunningham, J.Bailin, and C. Faucher-Giguere. The galaxy progenitors of stellar streams around milky way-mass galaxies in the fire cosmological simulations. 2021. https://doi.org/10.48550/arXiv.2104.09660.

P. Sharda, M. R. Krumholz, E. Wisnioski, J. C. Forbes, C. Federrath, and A. Acharyya. The physics of gas-phase metallicity gradients in galaxies. 2021. https://doi.org/10.48550/arXiv.2102.01234.

N. Shipp, D. Erkal, A Drlica-Wagner, T. S. Li, A. B. Pace, S. E. Koposov, L. R. Cullinane, G. S. Da Costa, A. P. Ji, K. Kuehn, G. F. Lewis, D. Mackey, J.D.Simpson, Z. Wan, D. B. Zucker, J. Bland-Hawthorn, P. S. Ferguson, S. Lilleengen, and S5 Collaboration. Measuring the mass of the large magellanic cloud with stellar streams observed by s5. *The Astronomical Journal, Volume 923, Number 2*, 2021. https://doi.org/10.3847/1538-4357/ac2e9.

N. Shipp, N. Panithanpaisal, L. Necib, D. Erkal R. Sanderson, T. S. Li, I. B. Santistevan, A. Wetzel, A. P. Ji L. R. Cullinane, S. E. Koposov, K. Kuehn, G. F. Lewis, A. B. Pace, D. B. Zucker, J. Bland-Hawthorn, E. C. Cunningham, S. Y. Kim, S. Lilleengen, J. Moreno, S. Sharma, S5 Collaboration, and FIRE Collaboration. S5: Probing the milky way and magellanic clouds potentials with the 6d map of the orphan-chenab stream. *The Astronomical Journal, Volume 949, Number 2*, 2023. https://doi.org/10.3847/1538-4357/acc582.

E. Vasiliev, V. Belokurov, and D. Erkal. Tango for three: Sagittarius, lmc, and the milky way. *Monthly Notices of the Royal Astronomical Society, Volume 501, Issue 2, pp.2279-2304*, 2020. https://doi.org/10.48550/arXiv.2009.10726.

A Appendix

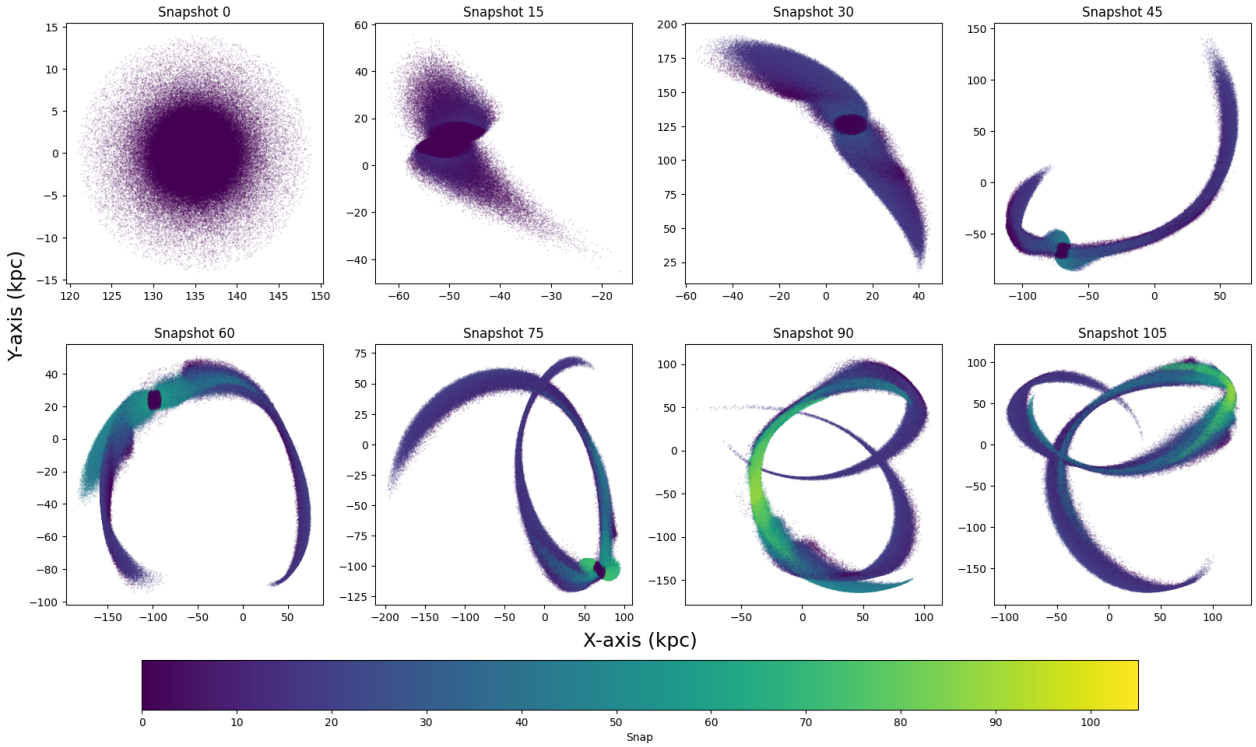

Figure 18: A figure to show the progressive dissolution of the stars for 105 snapshots with 1 million years each.

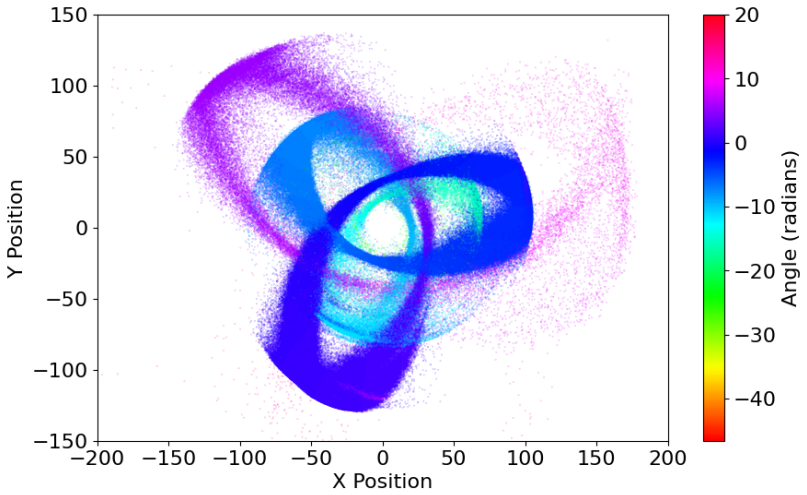

Figure 19: A figure showing the unwrapped stellar stream of a dwarf galaxy after 14 Gyr of evolution. Observing how the dark matterr present in the dwarf galaxy allows for a slower rate of disruption, hence the method works for longer periods and stars extend over a larger angular distance.

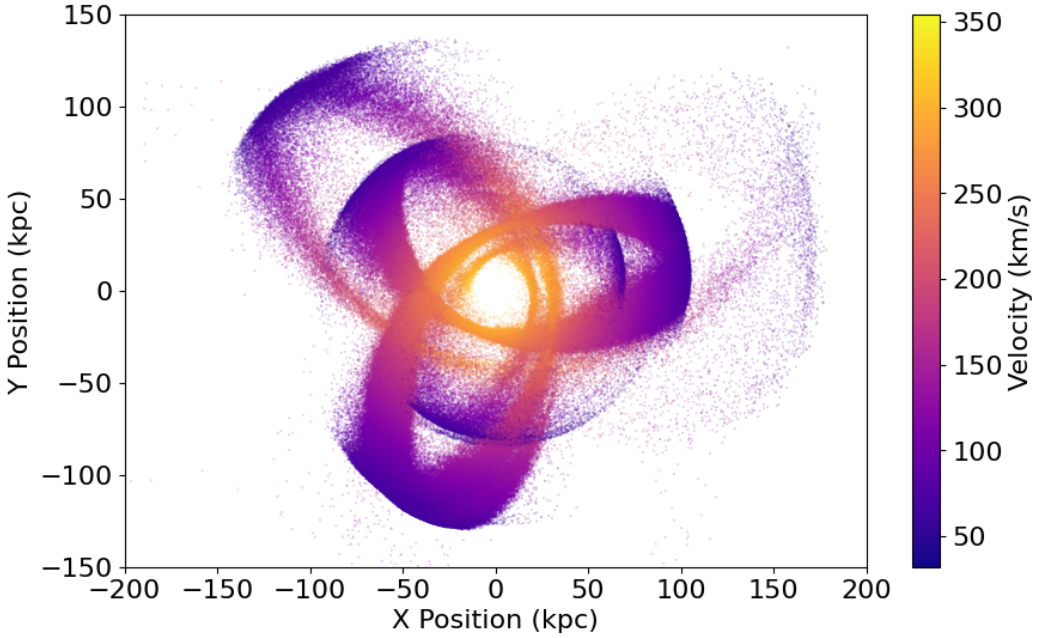

Figure 20: A figure showing the velocity distribution in stars of a stellar stream of a dwarf galaxy after 14 Gyr of evolution.

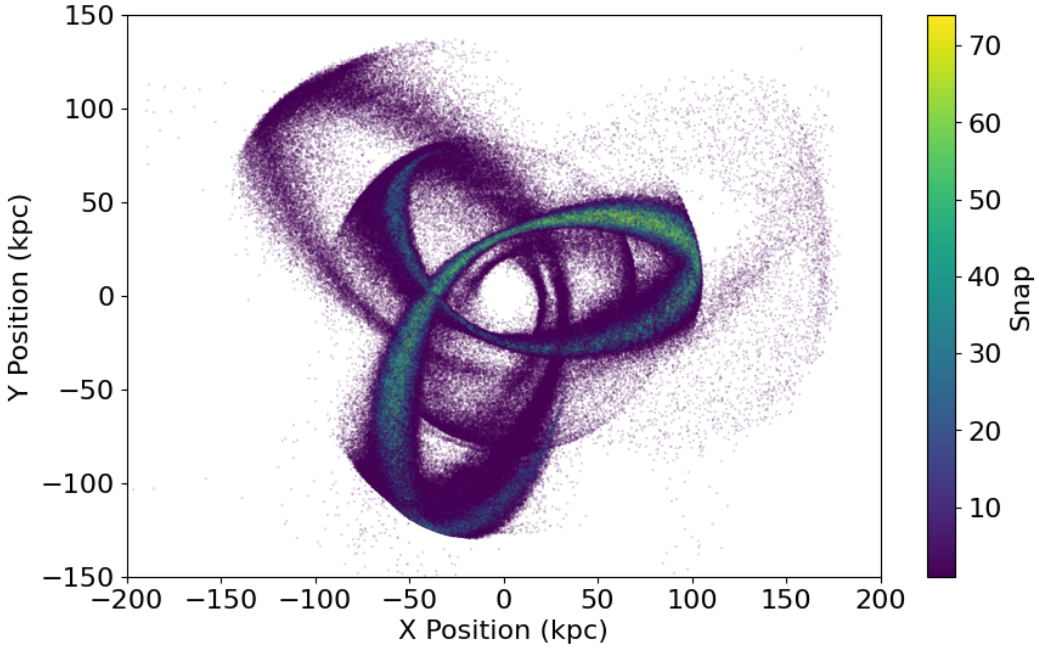

Figure 21: A figure showing the points in time where stars are shed from the progenitor of a stellar stream of a dwarf galaxy after 14 Gyr of evolution where each snapshot represents 0.1 Gyr.